

Mirroring the Parking Target: An Optimal-Control-Based Parking Motion Planner with Strengthened Parking Reliability and Faster Parking Completion*

Jia Hu, Yongwei Feng, Shuoyuan Li, Haoran Wang

Abstract—Automated Parking Assist (APA) systems are now facing great challenges of low adoption in applications, due to users’ concerns about parking capability, reliability, and completion efficiency. To upgrade the conventional APA planners and enhance user’s acceptance, this research proposes an optimal-control-based parking motion planner. Its highlight lies in its control logic: planning trajectories by mirroring the parking target. This method enables: i) parking capability in narrow spaces; ii) better parking reliability by expanding Operation Design Domain (ODD); iii) faster completion of parking process; iv) enhanced computational efficiency; v) universal to all types of parking. A comprehensive evaluation is conducted. Results demonstrate the proposed planner does enhance parking success rate by 40.6%, improve parking completion efficiency by 18.0%, and expand ODD by 86.1%. It shows its superiority in difficult parking cases, such as the parallel parking scenario and narrow spaces. Moreover, the average computation time of the proposed planner is 74 milliseconds. Results indicate that the proposed planner is ready for real-time commercial applications.

I. INTRODUCTION

In 2021, the global Automated Parking Assist (APA) system market is 10.1 billion USD [1]. The penetration rate of APA has reached a high level of 12.3% [2]. However, the user acceptance rate of APA is still quite low, as it is the third least-used application among all thirty-three Advanced Driver Assistance Systems (ADAS) functions, according to *Driver Interactive Vehicle Experience Report* [3]. There are two critical reasons. First, current APA systems are with low success rate, since they can hardly handle narrow spaces [4]. Second, current APA systems are time-consuming due to higher computation time and more “D-R” gear shiftings. Therefore, existing APA systems need to be further enhanced.

Generally, the APA system consists of three modules: perception, planning, and control. A centimeter-level perception has already been realized by high-precision sensors and environment recognition algorithms. Moreover, control methods are also with high accuracy. State-of-the-art control error is less than 5cm [5, 6]. Therefore, perception and

control are ready for the commercialization of APA [4]. The key to enhancing the existing APA system is the development of an APA planner.

There are mainly three types of parking planners, including geometry-based planners, search-based planners, and optimal-control-based planners.

Geometry-based planners formulate paths by connecting the starting position with the target position through geometric lines. Geometry-based planners consist of customized planners and fixed-library planners. Customized planners are proposed at the earliest, such as spline curve [7, 8]. However, they cannot consider vehicle dynamics. Sometimes it is impossible for the vehicle to trace the planned curve. It would decrease the execution success rate. To address this problem, fixed-library planners are proposed, such as reeds-sheep curve [9, 10]. The parking path is formulated by selecting and combining curves retrieved from a fixed library. All curves in the fixed library meet the requirement of vehicle dynamics. However, its planning domain is greatly limited because of its fixed nature. The shortcoming becomes critical especially in narrow spaces, as it can hardly plan a parking path. Therefore, the parking success rate of geometry-based planners is always a concern.

Search-based planners generate paths by searching a feasible path on a map [11, 12]. The map is divided into grids. Then the search process is conducted by exploring, picking, and connecting grid points. However, the computation efficiency reduces with the increase of environment complexity. In a complex environment, a smaller grid is needed to model the boundary of numerous irregular obstacles. It significantly increases the number of grids on the map and further increases search time [13]. Past studies show that even minutes are needed to find a parking path with search-based planners. Therefore, search-based planners can not ensure real-time application.

Optimal-control-based planners generate paths by solving optimization problems [14, 15]. They could output detailed motion commands, such as acceleration and steering angle, with the consideration of vehicle dynamics. It enables the vehicle to precisely trace a planned curve. However, optimal-control-based planners are still concerned with the time-consuming problem due to frequent “D-R” gear shiftings. To reach a target position in a narrow space, the final state error cost is given with a great weighting factor. It makes the planner short-sighted. The planned path would fast arrive at the vicinity of the target position and then oscillate around it, as shown in Fig. 1. Oscillating path leads to multiple driving direction switchings, which reduce driving

*This paper is partially supported by National Key R&D Program of China (2022YFF0604905), Shanghai Automotive Industry Science and Technology Development Foundation (No. 2213), and Tongji Zhongte Chair Professor Foundation (No. 000000375-2018082). (Corresponding author: Haoran Wang)

Jia Hu, Yongwei Feng, Shuoyuan Li, and Haoran Wang are with Key Laboratory of Road and Traffic Engineering of the Ministry of Education, Tongji University, Shanghai, China, 201804, (e-mail: hujia@tongji.edu.cn; 2210176@tongji.edu.cn; wang_haoran@tongji.edu.cn; 2131304@tongji.edu.cn).

comfortability and increase parking completion time. Therefore, a new planner is needed to minimize the number of driving direction switchings.

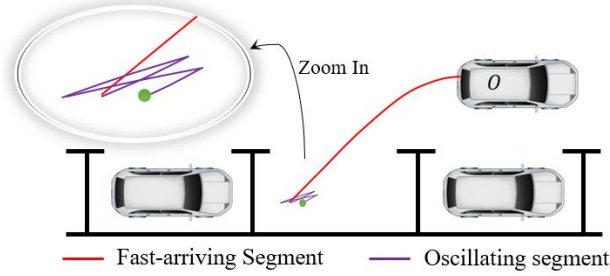


Fig. 1. Conventional parking path planning results

Besides the concerns on parking success rate and parking completion time, all past studies lack a clear Operation Design Domain (ODD). A clear ODD is quite crucial for the commercialization of APA to understand where an APA system is functional [16].

Therefore, a novel parking motion planner is proposed in this paper to address the above problems. It is with the following features:

- With parking capability in narrow spaces
- With better parking reliability by expanding ODD
- With faster completion of parking process
- With enhanced computational efficiency
- Universal to all types of parking

The remainder of this paper is organized as follows. Section II proposes the methodology of this paper. Section II.E verifies the proposed motion planner using simulation. Section IV draws a conclusion and provides future research discussion.

II. METHODOLOGY

The highlight of the proposed motion planner lies in its logic: mirroring the parking target. Conventionally, a parking motion planner aims at generating paths towards the target parking slot. It is with a great planning complexity, since the driving direction switching may be a must, as illustrated in Fig. 2(a). By proving the equivalence between reverse-driving and forward-driving, a reverse-and-forward maneuver can be transformed into a monodirectional maneuver, as shown in Fig. 2(b). This maneuver is achieved by planning towards a mirrored parking target, as shown in Fig. 2(b). It is exactly the proposed method. This method enhances the parking performance from the following perspectives:

• **Enhancing computational efficiency:** By transforming conventional reverse-and-forward planning into monodirectional planning, the planning domain of speed is reduced (no negative speed). As a result, the solution space is consequently reduced. Hence, computational efficiency is greatly enhanced.

• **Enhancing parking capability in narrow spaces:** Conventional parking motion planners are mostly short-sighted. They aim at fast arriving at the vicinity of the target position. There may not be enough space for adjustments around the target position in a narrow slot. While, by mirroring the parking target, the proposed motion planner

is global optimality oriented. As shown in Fig. 2 (b), the reverse driving segment would make space for the forward driving segment. It would enhance the parking success rate in narrow spaces.

• **Accelerating parking process:** Since the proposed motion planner is with global optimality, oscillations around the target position can be reduced, as shown in Fig. 1. Hence, the number of driving direction switching is minimized. This ensures faster parking completion.

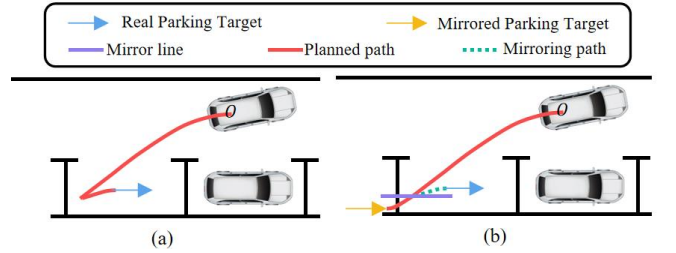


Fig. 2. Example of mirrored parking target

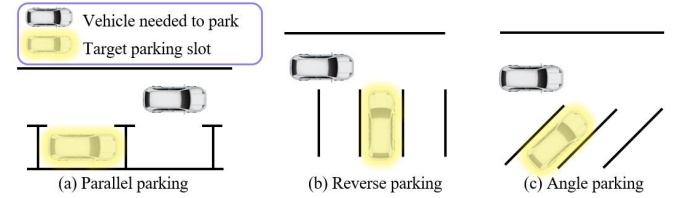


Fig. 3. Three types of parking

A. Control Logic

The purpose of this paper is to propose an optimal-control-based motion planner. Scenarios of interest are illustrated in Fig. 3, including parallel, reverse, and angle parking scenarios.

The parking system is presented in Fig. 4. It consists of 5 modules. Module 1 senses the surrounding environment. Module 2 determines the position of the mirror line. Module 3 makes planning decisions. Module 4 plans trajectories and outputs control commands. Module 5 is an execution layer. Details of this system are provided as follows:

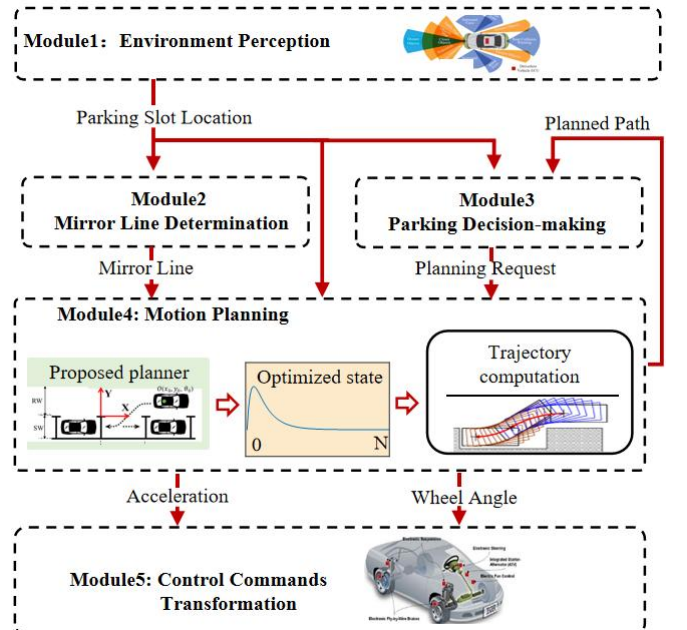


Fig. 4. Parking system

- Module 1: This module collects the location of the parking slot.
- Module 2: The mirror line is determined in this module for all types of parking scenarios, as shown in Fig. 5. It is used for determining a mirrored parking target, so that reverse-and-forward planning could be transformed into monodirectional planning.

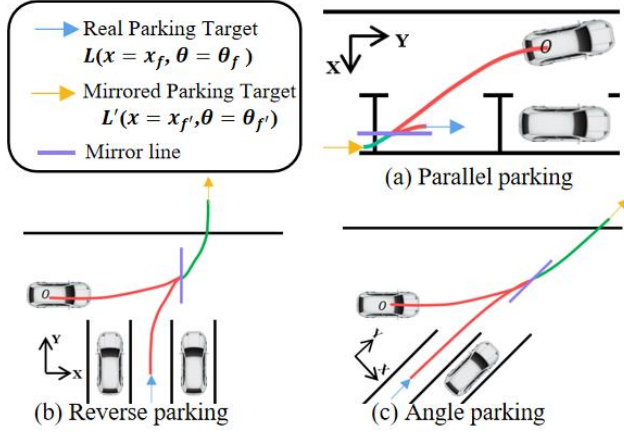


Fig. 5 Definition of the mirror line

- Module 3: This module conducts decision-making in the parking processes. It outputs planning requests which would activate Module 4.
- Module 4: This module plans parking trajectories towards the mirrored parking target. The planned motion commands, including acceleration and steering angle, are passed to module 5.
- Module 5: Control commands provided by Module 4 control the vehicle towards the mirrored parking target. This module transforms the control commands to control the vehicle towards the real parking target, as shown in Fig. 6.

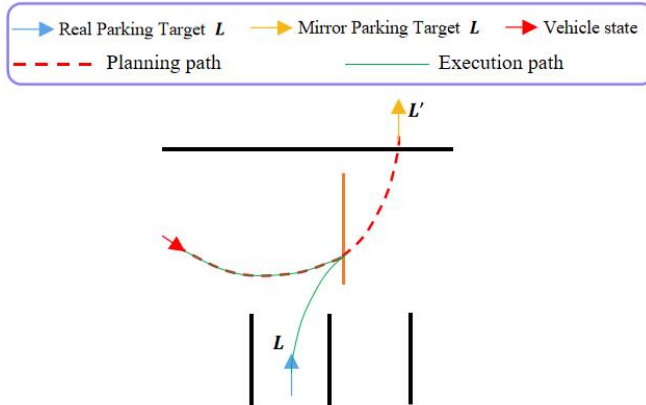


Fig. 6 Example of control commands transformation

TABLE I lists the indices and parameters utilized hereafter.
TABLE I Indices and parameters

Parameter	Description
a	Acceleration (m/s^2)
a_{com}	Commanded acceleration (m/s^2)
a_{min}	Minimum acceleration (m/s^2)
a_{max}	Maximum acceleration (m/s^2)
a_l^k	Coefficient of the l_{th} edge of R_{if}^k .
A	Coefficient matrix in vehicle dynamics model
B	Coefficient matrix in vehicle dynamics model
b_l^k	Coefficient of the l_{th} edge of R_{if}^k .

c_l^k	Coefficient of the l_{th} edge of R_{if}^k .
f	The full problem
φ	Heading angle with respect to x direction (rad)
i	Step in prediction horizon
J	Cost function of the full problem
K	The number of infeasible regions
l	Distance between rear axle and front axle (m)
l_1	Distance between rear axle and the rear most part of the vehicle (m)
l_2	Distance between rear axle and the front most of the vehicle (m)
l_3	Vehicle width (m)
M	A large enough number in the big M method
N	Total control steps
Q	Weighting factor of state error in the motion planner
r_{min}	Vehicle's minimum turning radius (m)
R	Weighting factor of control penalty in the motion planner
R_{if}^k	k_{th} infeasible region
RW	Road Width (m)
SL	Length of parking slot (m)
SW	Width of parking slot (m)
t	Time (seconds)
u	Control vector of vehicle
v	Vehicle speed (m/s)
v_{min}	Minimum vehicle speed (m/s)
v_{max}	Maximum vehicle speed (m/s)
x	Center of vehicle rear axle in x direction (m)
y	Center of vehicle rear axle in y direction (m)
x_f	Coordinate of real parking target in x direction (m)
x_f'	Coordinate of mirrored parking target in x direction (m)
x_{p^m}	Coordinate of m_{th} feature point in x direction (m)
y_{p^m}	Coordinate of m_{th} feature point in y direction (m)
z_l^k	Binary variable in big M method
β	Tire slip angle (rad)
θ	Vehicle's heading angle (rad)
θ_f	Angle of real parking target (rad)
θ_f'	Angle of mirrored parking target (rad)
δ_f	Front-wheel angle (rad)
$\delta_{f,com}$	Commanded front-wheel angle (rad)
$\delta_{f,min}$	Minimum front-wheel angle (rad)
$\delta_{f,max}$	Maximum front-wheel angle (rad)
ξ	State vector of vehicle
ξ_{des}	Desired state vector of vehicle
Δt	Discrete time step size (seconds)
τ_{δ_f}	First-order inertia delay of steering (seconds)
τ_a	First-order inertia delay of acceleration (seconds)
Θ	A set of steps with collision avoidance constraints

B. Mirror Line Determination

In this section, a mirror line determination method is proposed for all types of parking scenarios.

1) Parallel parking

Theorem 1: Considering target reachability and collision avoidance, in parallel parking scenarios, the distance between the mirror line and the real parking target l_{mi} shall be constrained by Eqs. (1) and (2).

$$l_{mi} \geq r_{min} * (1 - \cos \theta) \quad (1)$$

$$l_{mi} \leq \frac{SW}{2} - l_1 * \sin \theta - \frac{l_3}{2} * \cos \theta \quad (2)$$

where l_{mi} is the distance between the mirror line and the real parking target. r_{min} is the vehicle's minimum turning radius. θ is the vehicle's heading angle. l_1 is the distance between rear axle and the rear end of the vehicle. l_3 is vehicle width.

Proof:

At the position of mirror line, the vehicle shall be able to reach the real parking target within its turning capacity, in order to ensure target reachability. Considering the vehicle's minimum turning radius is r_{min} and the vehicle heading is θ , Eq. (1) is obtained based on geometric relations, as shown in Fig. 7(a).

To ensure collision avoidance, the bottom corner of the vehicle (pink point) should not collide with the parking slot, when the vehicle arrives at the mirror line, as shown in Fig. 7(b). Based on geometric relations, l is deduced as Eq. (3):

$$l = l_1 * \sin \theta - \frac{l_3}{2} * \cos \theta \quad (3)$$

To avoid collisions, Eq. (4) should be satisfied.

$$l + l_{mi} < \frac{SW}{2} \quad (4)$$

By substituting Eq. (3) into Eq. (4), Eq. (2) is obtained. This concludes the proof. ■

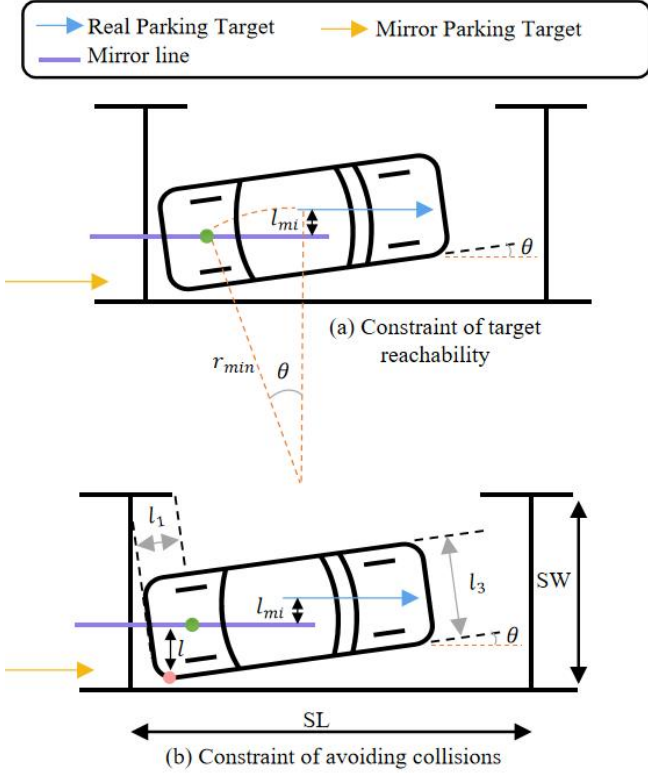


Fig. 7 Mirror line of parallel parking

Based on Theorem 1, the feasible domain of mirror position l_{mi} is illustrated in Fig. 8. l_{mi} is correlated with the vehicle heading angle. The blue line is the upper boundary. The red line is the lower boundary. The overlap is the feasible domain. Moreover, to ensure greater robustness on the heading angle, the dark point is suggested in practical applications.

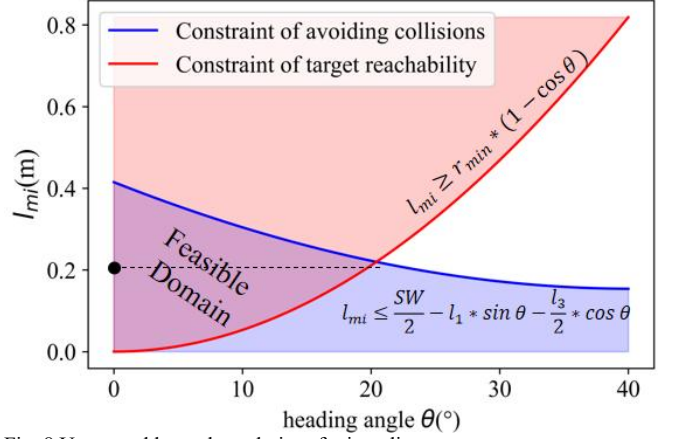


Fig. 8 Upper and lower boundaries of mirror line

2) Reverse parking

Simpler than parallel parking, the vehicle trajectory leading towards a reverse parking slot has only one requirement in the vicinity of the mirror line: when the vehicle is on the mirror line, it should be able to park into the slot directly within its turning capacity. The collision avoidance requirement no longer stands, as a vehicle would never bump into the boundary of a parking slot at the position of a mirror line. Hence, according to geometric relations, the distance between the mirror line and the real parking target l_{mi} shall be constrained by Eq. (5). A mirror line could be determined according to users' preferences as long as the constraint is satisfied.

$$l_{mi} \geq r_{min} * (1 - \cos(\frac{\pi}{2} - \theta)) \quad (5)$$

where l_{mi} is the distance between the mirror line and the real parking target. r_{min} is the vehicle's minimum turning radius. θ is the vehicle's heading angle.

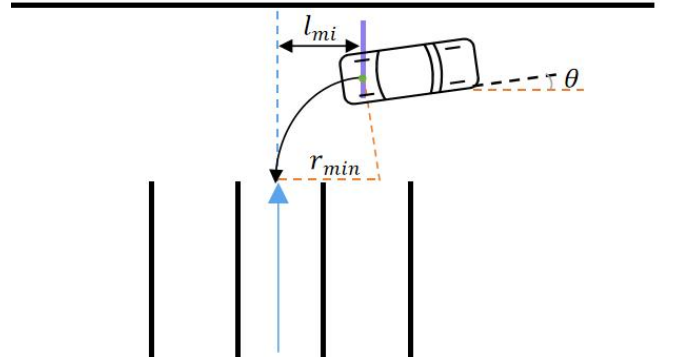


Fig. 9 Mirror line of reverse parking

3) Angle parking

Similar to reverse parking, as shown in Fig. 10, the distance between the mirror line and the real parking target l_{mi} shall be constrained by Eq. (6), to ensure target reachability.

$$l_{mi} \geq r_{min} * (1 - \cos(\frac{\pi}{4} - \theta)) \quad (6)$$

where l_{mi} is the distance between the mirror line and the real parking target. r_{min} is the vehicle's minimum turning radius. θ is the vehicle's heading angle.

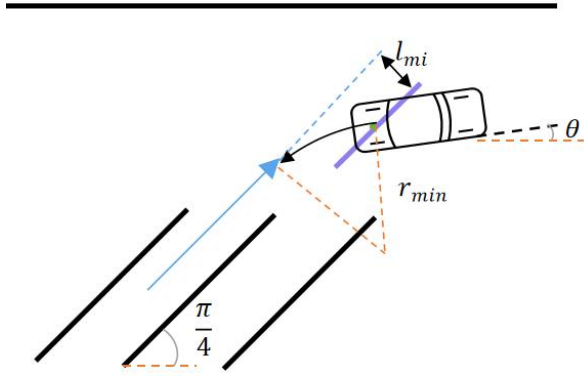
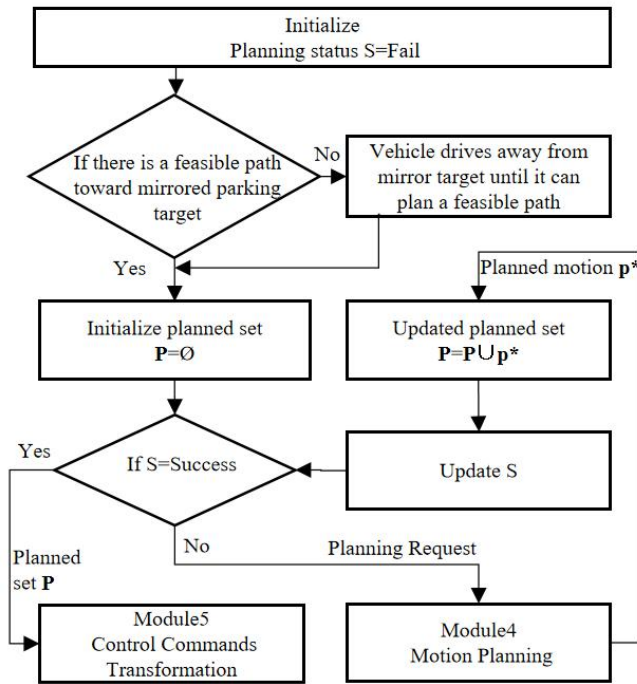


Fig. 10 Mirror line of angle parking

C. Parking Decision-making

In the parking maneuver, the vehicle may not park into the slot within one direction switching, especially in narrow spaces. Hence, the decision-making is needed to generate requests on parking planning. A parking decision-making algorithm is proposed as shown in TABLE II.

TABLE II Parking decision-making algorithm



D. Motion Planning Problem Formulation

The formulation of motion planning is presented in this section.

1) Proof of equivalence between Reverse-driving and Forward-driving

This section proves the equivalence between reverse-driving and forward-driving as shown in **Theorem 2**. By proving it, a reverse-and-forward maneuver can be transformed into a monodirectional maneuver.

Theorem 2: It is assumed that two vehicles are at the same position on mirror line and have opposite driving direction, as shown in Eq. (7) and Fig. 11. By executing opposite control commands in Eq. (8), the mirrored path of forward-driving

vehicle is symmetric to the planned path of reverse-driving vehicle, as shown in Eq. (9).

$$\begin{cases} x_{back}(0) = x_{forth}(0) = 0 & (a) \\ y_{back}(0) = y_{forth}(0) = 0 & (b) \\ \theta_{back}(0) = \theta_{forth}(0) & (c) \\ v_{back}(0) = -v_{forth}(0) & (d) \end{cases} \quad (7)$$

where x , y , and θ represent the location and heading angle of the vehicle. v represents the vehicle's speed. The subscript back and forth represent the reverse-driving vehicle and the forward-driving vehicle respectively. 0 represents the initial time.

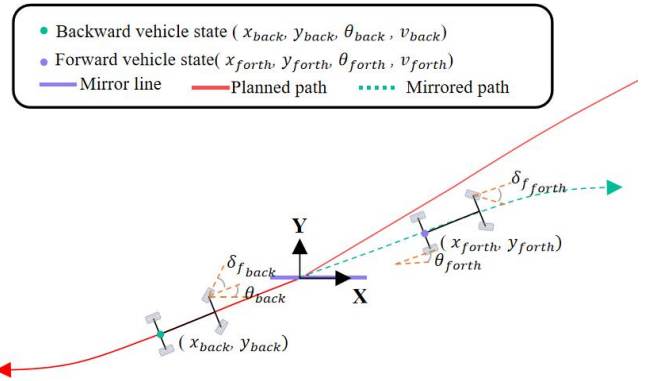


Fig. 11 Reverse-driving and Forward-driving vehicle

$$\begin{cases} \delta_{f_{forth}}(t) = -\delta_{f_{back}}(t) & (a) \\ a_{forth}(t) = -a_{back}(t) & (b) \end{cases} \quad (8)$$

$$\begin{cases} x_{back}(t) = -x_{forth}(t) & (a) \\ y_{back}(t) = -y_{forth}(t) & (b) \\ \theta_{back}(t) = \theta_{forth}(t) & (c) \\ v_{back}(t) = -v_{forth}(t) & (d) \end{cases} \quad (9)$$

Proof:

The vehicle dynamics are generally modeled by a kinematic bicycle model as follows [17].

$$\begin{cases} \dot{x} = v * \cos \theta \\ \dot{y} = v * \sin \theta \\ \dot{\theta} = \frac{v * \tan \delta_f}{l} \\ \dot{v} = a \end{cases} \quad (10)$$

where x and y represent the center of the vehicle's rear axle. v is the vehicle's speed. Its direction is the direction of the car body. θ is the heading angle with respect to x direction. l is the distance between rear axles and front axles. δ_f and a are control commands. They are front-wheel angle and acceleration respectively.

Applying opposite control commands into Eq. (10), the states of the two vehicles propagate as shown in Eqs. (11) and (12):

$$\begin{cases} x_{forth}(t) = x_{forth}(0) + \int_0^t v_{forth}(\tau) * \cos \theta_{forth}(\tau) d\tau & (a) \\ y_{forth}(t) = y_{forth}(0) + \int_0^t v_{forth}(\tau) * \sin \theta_{forth}(\tau) d\tau & (b) \\ \theta_{forth}(t) = \theta_{forth}(0) + \int_0^t \frac{v_{forth}(\tau) * \tan \delta_{forth}(\tau)}{l} d\tau & (c) \\ v_{forth}(t) = v_{forth}(0) + \int_0^t a_{forth}(\tau) d\tau & (d) \end{cases} \quad (11)$$

$$\begin{cases} x_{back}(t) = x_{back}(0) + \int_0^t v_{back}(\tau) * \cos \theta_{back}(\tau) d\tau & (a) \\ y_{back}(t) = y_{back}(0) + \int_0^t v_{back}(\tau) * \sin \theta_{back}(\tau) d\tau & (b) \\ \theta_{back}(t) = \theta_{back}(0) + \int_0^t \frac{v_{back}(\tau) * \tan \delta_{back}(\tau)}{l} d\tau & (c) \\ v_{back}(t) = v_{back}(0) + \int_0^t a_{back}(\tau) d\tau & (d) \end{cases} \quad (12)$$

Based on Eq. (8)(b), Eq. (13) is obtained.

$$\int_0^t a_{back}(\tau) d\tau = - \int_0^t a_{forth}(\tau) d\tau \quad (13)$$

By substituting Eq. (13) and Eq (7)(d) into Eq. (12)(d), Eq. (14) is obtained.

$$v_{back}(t) = - \left(v_{forth}(0) + \int_0^t a_{forth}(\tau) d\tau \right) \quad (14)$$

By substituting Eq. (11)(d) into Eq. (14), Eq. (15) is obtained.

$$v_{back}(t) = - v_{forth}(t) \quad (15)$$

Similarly, by substituting Eq (7), Eq. (8)(a), and Eq. (15) into Eq. (11) and Eq. (12), Eq. (16) is obtained.

$$\theta_{back}(t) = \theta_{forth}(t) \quad (16)$$

By substituting Eq. (15) and Eq. (16) into Eq. (11)(a-b) and Eq. (12)(a-b), Eq. (17) is obtained.

$$\begin{cases} \int_0^t v_{forth}(\tau) \cos \theta_{forth}(\tau) d\tau = - \int_0^t v_{back}(\tau) \cos \theta_{back}(\tau) d\tau \\ \int_0^t v_{forth}(\tau) \sin \theta_{forth}(\tau) d\tau = - \int_0^t v_{back}(\tau) \sin \theta_{back}(\tau) d\tau \end{cases} \quad (17)$$

By substituting Eq (7)(a-b) and Eq. (17) into Eq. (11)(a-b) and Eq. (12)(a-b), Eq. (18) is obtained.

$$\begin{cases} x_{back}(t) = - x_{forth}(t) & (a) \\ y_{back}(t) = - y_{forth}(t) & (b) \end{cases} \quad (18)$$

By combining Eq. (15), Eq. (16), and Eq. (18), Eq. (9) is obtained.

It shows that the mirrored path of forward-driving vehicle is symmetric to the planned path of reverse-driving vehicle. Therefore, Theorem 2 is concluded. ■

2) State Definition

State and control vectors are defined in **Definition 1** and **Definition 2**.

Definition 1: Vehicle state vector ξ and control vector \mathbf{u} are defined as follows:

$$\xi \stackrel{\text{def}}{=} [x(i), v(i), a(i), y(i), \theta(i), \delta_f(i)]^T \quad (19)$$

$$\mathbf{u} \stackrel{\text{def}}{=} [a_{com}(i), \delta_{f_{com}}(i)]^T \quad (20)$$

Definition 2: Desired vehicle state vector ξ_{des} are defined as follows.

$$\xi_{des} \stackrel{\text{def}}{=} [x_{f'}, 0, 0, \sim, \theta_{f'}, 0]^T \quad (21)$$

where $x_{f'}$ is the coordinate of the mirrored parking target in x direction. $\theta_{f'}$ is the heading angle of the mirrored parking target.

3) System Dynamics

Discrete vehicle dynamics are formulated by adopting a linearized bicycle model [18-20] as follows:

$$x_{i+1} = x_i + v_i \times \Delta t \quad (22)$$

$$y_{i+1} = y_i + v_i \times \theta_i \times \Delta t \quad (23)$$

$$\theta_{i+1} = \theta_i + v_i \times \frac{\delta_{f_i}}{l} \times \Delta t \quad (24)$$

$$v_{i+1} = v_i + a_i \times \Delta t \quad (25)$$

where l is the distance between rear axles and front axles. Δt is the discrete time step size.

To model the local control response accurately, vehicle control delay is considered by a first-order inertia model as follows:

$$a_{i+1} = a_i + \frac{a_{com_i} - a_i}{\tau_a} \times \Delta t \quad (26)$$

$$\delta_{f_{i+1}} = \delta_{f_i} + \frac{\delta_{f_{com_i}} - \delta_{f_i}}{\tau_{\delta_f}} \times \Delta t \quad (27)$$

where τ_{δ_f} and τ_a are the first-order inertia delay of steering and acceleration respectively.

By applying the Eqs. (22)-(27) into Eqs. (19)-(20), vehicle dynamics models are formulated as follows.

$$\xi_{i+1} = \mathbf{A}_i \xi_i + \mathbf{B}_i \mathbf{u}_i \quad (28)$$

$$\mathbf{A}_i = \Delta t \times \begin{bmatrix} 0 & 0 & 0 & 0 & 0 \\ 0 & 1 & 0 & 0 & 0 \\ 0 & -\frac{1}{\tau_a} & 0 & 0 & 0 \\ 0 & 0 & 0 & v & 0 \\ 0 & 0 & 0 & 0 & \frac{v}{l} \\ 0 & 0 & 0 & 0 & -\frac{1}{\tau_{\delta_f}} \end{bmatrix} + \mathbf{I}_{6 \times 6} \quad (29)$$

$$\mathbf{B}_i = \Delta t \times \begin{bmatrix} 0 & 0 \\ 0 & 0 \\ 1 & 1 \\ \tau_a & \tau_{\delta_f} \end{bmatrix} \quad (30)$$

4) Cost Function

To accelerate computation, cost functions are both formulated into a quadratic form. The objective function is formulated as follows:

$$\min_{\mathbf{u}} \left(\sum_{i=1}^N \left(\underbrace{\mathbf{Q} \|\xi_i - \xi_{des}\|_2}_{\text{State error cost}} + \underbrace{\mathbf{R} \|u_i\|_2}_{\text{Control cost}} \right) + \underbrace{\mathbf{Q} \|\xi_{N+1} - \xi_{des}\|_2}_{\text{Terminal state error cost}} \right) \quad (31)$$

where $\mathbf{Q}\|\xi_i - \xi_{des}\|_2$ is the state error cost. $\mathbf{R}\|u_i\|_2$ is control effort cost. Weighting factors of state error cost \mathbf{Q} is a positive-definite matrix. Weighting factors of control effort cost \mathbf{R} is also a positive-definite matrix.

5) Constraints

a) *State and Control Constraint*: Vehicle speed should be constrained within speed limits. Vehicle's acceleration should be bounded by vehicle capability and comfort. Vehicle's front wheel angle should be within its steering range.

$$v_{min} \leq v \leq v_{max} \quad (32)$$

$$a_{min} \leq a \leq a_{max} \quad (33)$$

$$\delta_{f_{min}} \leq \delta_f \leq \delta_{f_{max}} \quad (34)$$

where v_{min} and v_{max} are the minimum and maximum vehicle speed respectively. a_{min} and a_{max} are the minimum and maximum acceleration respectively. $\delta_{f_{min}}$ and $\delta_{f_{max}}$ are minimum and maximum front-wheel angle respectively.

b) *Constraints on Vehicle State on the Mirror Line*: The vehicle would switch its driving direction at the position of the mirror line. Therefore, the speed must be zero on the mirror line.

$$v_i = 0 \text{ if } |x_i - l_1| \leq \varepsilon \quad (35)$$

where ε is a small positive number.

c) *Obstacles Avoidance Constraint*: To avoid collisions, the ego vehicle should be outside all infeasible parking regions R_{if}^k , as shown in Fig. 13. Six feature points are selected to represent the ego vehicle, as shown in Fig. 12. Coordinates of feature points are computed in Eq. (36) as follows.

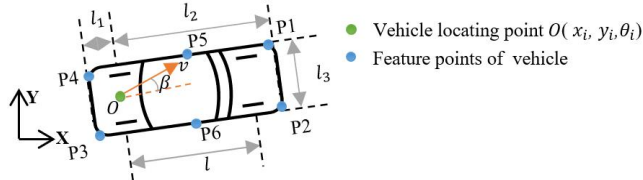


Fig. 12. Illustration of notations

$$\left\{ \begin{array}{l} x_{p_i^1} = x_i + l_2 * \cos \theta_i - \frac{l_3}{2} * \sin \theta_i \\ y_{p_i^1} = y_i + l_2 * \sin \theta_i + \frac{l_3}{2} * \cos \theta_i \\ x_{p_i^2} = x_i + l_2 * \cos \theta_i + \frac{l_3}{2} * \sin \theta_i \\ y_{p_i^2} = y_i + l_2 * \sin \theta_i - \frac{l_3}{2} * \cos \theta_i \\ x_{p_i^3} = x_i - l_1 * \cos \theta_i + \frac{l_3}{2} * \sin \theta_i \\ y_{p_i^3} = y_i - l_1 * \sin \theta_i - \frac{l_3}{2} * \cos \theta_i \\ x_{p_i^4} = x_i - l_1 * \cos \theta_i - \frac{l_3}{2} * \sin \theta_i \\ y_{p_i^4} = y_i - l_1 * \sin \theta_i + \frac{l_3}{2} * \cos \theta_i \\ x_{p_i^5} = x_i + \frac{(l_2 - l_1)}{2} * \cos \theta_i - \frac{l_3}{2} * \sin \theta_i \\ y_{p_i^5} = y_i + \frac{(l_2 - l_1)}{2} * \sin \theta_i + \frac{l_3}{2} * \cos \theta_i \\ x_{p_i^6} = x_i + \frac{(l_2 - l_1)}{2} * \cos \theta_i + \frac{l_3}{2} * \sin \theta_i \\ y_{p_i^6} = y_i + \frac{(l_2 - l_1)}{2} * \sin \theta_i - \frac{l_3}{2} * \cos \theta_i \end{array} \right. \quad (36)$$

where $P_1(x_{p_i^1}, y_{p_i^1})$, $P_2(x_{p_i^2}, y_{p_i^2})$, $P_3(x_{p_i^3}, y_{p_i^3})$, $P_4(x_{p_i^4}, y_{p_i^4})$, $P_5(x_{p_i^5}, y_{p_i^5})$, and $P_6(x_{p_i^6}, y_{p_i^6})$ are the selected feature points.

The obstacle avoidance constraint could be formulated as follows.

$$(x_{p_i^m}, y_{p_i^m}) \notin R_{if}^k \quad (37)$$

$$\forall m \in \{1, 2, 3, 4, 5, 6\} \forall k \in \{1, 2, \dots, K\}$$

where p_i^m is m_{th} feature point. R_{if}^k is the k_{th} convex infeasible region as shown in Fig. 13.

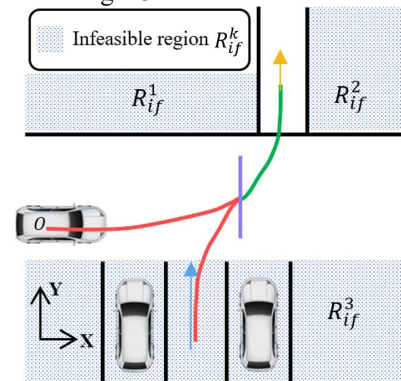


Fig. 13. Obstacles avoidance example

For the k_{th} convex infeasible region R_{if}^k , it can be represented by linear inequalities as shown in Eq. (38)

$$R_{if}^k \stackrel{\text{def}}{=} \bigcap_{l=1}^L a_l^k * x + b_l^k * y + c_l^k \leq 0 \quad (38)$$

where l represents the l_{th} edge of R_{if}^k . a_l^k , b_l^k and c_l^k are coefficients of the l_{th} edge of R_{if}^k .

By adopting the big M method [21], Eq. (37) is formulated as follows.

$$\bigcap_i \left\{ \begin{array}{l} \prod_{l=1}^L a_l^k * x_{p_i^m} + b_l^k * y_{p_i^m} + c_l^k \geq M * (1 - z_l^k) \\ \sum_{l=1}^L z_l^k \geq 1 \end{array} \right. \quad (39)$$

$\forall m \in \{1, 2, \dots, 6\} \forall k \in \{1, 2, \dots, K\} \forall i \in \Theta$

where M is a large enough number. z_l^k is a binary variable. Θ is a set that records which control steps need obstacle avoidance constraints.

6) Full problem

The full problem f is formulated as follows.

$$J \rightarrow \text{Eq. (31)}$$

s. t.

system dynamics \rightarrow Eqs. (28) – (30)

state and control constraint \rightarrow Eqs. (32) – (34)

mirror line constraint \rightarrow Eq. (35)

obstacles avoidance constraint \rightarrow Eq. (39)

Where J is the cost function of f .

7) Problem Solving

The proposed optimal-control-based motion planning problem is transformed into a Mixed Integer Quadratic Programming (MIQP) problem. The introduction of binary variables would decrease computational efficiency. Therefore, a novel design for computational efficiency enhancement is realized by an upper-layer iteration algorithm, as presented by TABLE III. In each cycle, the MIQP problem is solved by the Gurobi optimizer [22].

TABLE III Solving algorithm

Input: $R_{if} = \bigcup_{k=1}^K R_{if}^k, \forall k \in \{1, 2, \dots, K\}$

Initialize: the set of steps with collision avoidance constraints $\Theta = \emptyset$

Output: optimal parking trajectory P^*

get f according to Eq. (40) except Eq. (39)

$P^* = \text{MIQP}(f)$

While $P^* \cap R_{if} \neq \emptyset$ **then**

For $i \in \{0, 1, \dots, N\}$ **then**

If $P^*(i) \cap R_{if} \neq \emptyset$ **then**

$\Theta = \Theta \cup i$

End if

End For

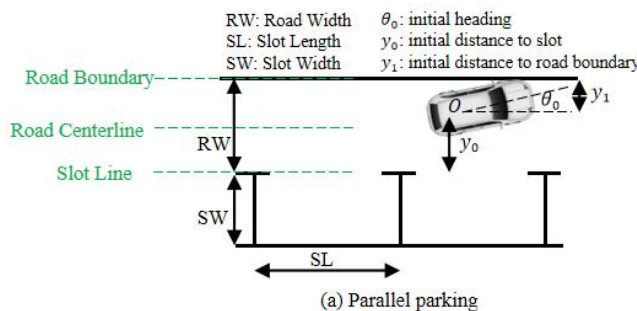
 update f according to Eq. (40)

$P^* = \text{MIQP}(f)$

End while

E. Control Commands Transformation

Based on Theorem 2, to control the vehicle towards the real parking target, the planned motion commands after the mirror line is executed oppositely, as shown in Eq. (41).



$$\begin{cases} \delta_{f_{executed}}(t) = -\delta_{f_{planned}}(t) & (a) \\ a_{executed}(t) = -a_{planned}(t) & (b) \end{cases} \quad (41)$$

where $\delta_{f_{planned}}$ and $a_{planned}$ is the planned control command. $\delta_{f_{executed}}$ and $a_{executed}$ is the executed control command.

III. EVALUATION

The proposed parking motion planner is evaluated from the following five aspects: i) function validation; ii) parking capability quantification; iii) parking reliability evaluation; iv) parking completion efficiency evaluation; v) computation efficiency evaluation.

A. Experiment Design

The experiment is conducted on a simulation platform previously developed by this research team [14, 23]. The following settings are adopted, as shown in TABLE IV.

TABLE IV Parameter settings

Parameter	Description	Settings
a_{min}	Minimum acceleration (m/s^2)	-5
a_{max}	Maximum acceleration (m/s^2)	3
l	Distance between rear axle and front axle (m)	2.5
l_1	Distance between rear axle and the rear most part of the vehicle (m)	0.71
l_2	Distance between rear axle and the rear most part of the vehicle (m)	3.11
l_3	Vehicle width (m)	1.67
N	Total control steps	60
v_{min}	Minimum vehicle speed (m/s)	-3
v_{max}	Maximum vehicle speed (m/s)	3
$\delta_{f_{min}}$	Minimum front-wheel angle (rad)	-0.6
$\delta_{f_{max}}$	Maximum front-wheel angle (rad)	0.6
Δt	Control step-size (seconds)	0.1
τ_{δ_f}	First-order inertia delay of steering (seconds)	0.1
τ_a	First-order inertia delay of acceleration (seconds)	0.3

1) Test Scenarios

The proposed motion planner is tested in three types of parking scenarios including parallel parking, reverse parking, and angle parking, as shown in Fig. 14. The vehicle is in a space comprised of slots and road. The slot size is determined by two factors: Slot Length (SL) and Slot Width (SW). Road Width (RW) indicates the distance between the parking slot and the road boundary. The vehicle would like to park into the slot from its initial position. The vehicle's initial position is defined by three factors: initial heading θ_0 , initial distance to slot y_0 , and initial distance to road boundary y_1 .

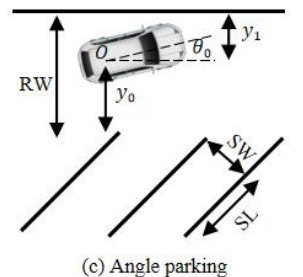
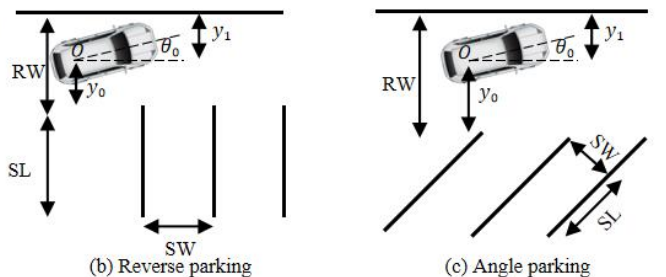


Fig. 14. Sensitive factors

2) Motion Planner Types

Two types of motion planners are evaluated:

- **Baseline planner:** This planner is a search-based planner [20, 24]. It is short-sighted due to its rationale that the planning is always towards the parking target.

- **The proposed planner:** This planner is optimal control based. It enhances parking performance due to its global optimality.

3) Measures of Effectiveness

The following Measures of Effectiveness (MOEs) are adopted.

a) Function Validation

Planned trajectories are used to verify the proposed function. The function of interest is mirroring the parking target.

b) Parking Capability in Narrow Spaces Quantification

The success rate of parking is used to quantify parking capability in narrow spaces. Criteria of a successful parking maneuver are defined according to ISO 16787 [25] and ISO 20900 [26] as follows.

i) **Criteria of Successful Parallel Parking:** As illustrated in Fig. 15, successful parallel parking requires that:

- Heading angle error θ is between -3° and 3° ;
- M_f , M_r , and M_e are all greater than 0;
- Parking time duration must be less than 180 seconds;
- No collisions;
- The vehicle outline is inside the parking slot.

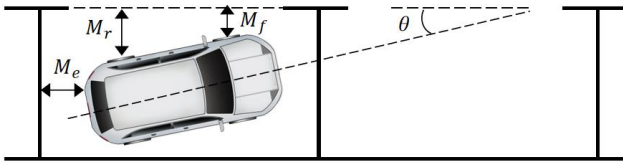
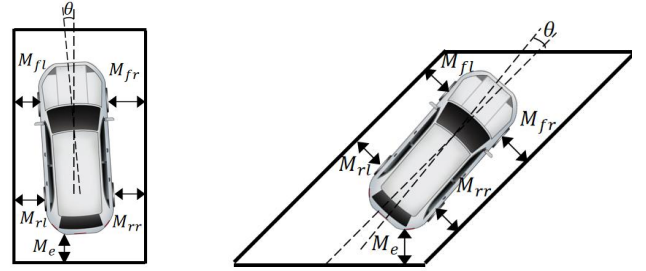


Fig. 15. Parallel parking example

ii) **Criteria of Successful Reverse and Angle Parking:** As illustrated in Fig. 16, successful reverse and angle parking require that.

- Heading angle error θ is between -3° and 3° ;
- M_{fl} , M_{fr} , M_{rl} , M_{rr} , and M_e are all greater than 0.1m;
- Parking time duration must be less than 180 seconds;

- No collisions;
- The vehicle outline is inside the parking slot.



(a) Reverse parking (b) Angle parking
Fig. 16. Reverse and angle parking example

c) Parking reliability Evaluation

ODD is used to evaluate parking reliability. ODD is a collection of initial conditions which could successfully complete the parking process with a rate of 95%. Initial conditions consist of the following factors: Slot Length (SL), Slot Width (SW), initial heading θ_0 , and initial distance to slot y_0 . A larger ODD indicates a more reliable parking planner.

d) Parking Completion Efficiency Evaluation

Parking completion efficiency is quantified by two measurements: the parking time duration and the number of driving direction switching [27].

e) Computation Efficiency Evaluation

The computation time of parking path planning is used to evaluate computation efficiency.

4) Sensitivity Analysis

The sensitivity analysis is conducted in terms of space size and initial position. Six factors in Fig. 14 are selected, including Road Width (RW), Slot Length (SL), Slot Width (SW), vehicle's initial heading θ_0 , vehicle's initial distance to slot y_0 , and vehicle's initial distance to road boundary y_1 . Levels of factors are set in TABLE V, according to ISO 16787 (*Assisted parking system — Performance requirements and test procedures*) [25] and ISO 20900 (*Partially automated parking systems — Performance requirements and test procedures*) [26]. By iterating through factor levels and excluding the cases unable to be generated, there are 71,009 cases, including 12995 parallel parking cases, 46629 reverse parking cases, and 11385 angle parking cases.

TABLE V Cases Design

Types of Parking	Road Width (RW)	Parking slot size		Initial heading θ_0	Initial distance to slot y_0
		Length (SL)	Width (SW)		
Parallel parking	4.5m	Minimum: 3.82m Maximum: 7.35m Sampling step: 0.1m	2.5m	Minimum: -90deg Maximum: 90deg Sampling step: 10deg	Minimum: 0m Maximum: Road Width Sampling step: 0.1m
	4.0m				
	3.5m				
Reverse parking	7m	4.82m	Minimum: 1.67m Maximum: 3.27m Sampling step: 0.05m	Minimum: -90deg Maximum: 90deg Sampling step: 10deg	Minimum: 0m Maximum: Road Width Sampling step: 0.1m
	6m				
	5m				
Angle parking	4.5m	4.82m	Minimum: 1.67m Maximum: 3.27m Sampling step: 0.05m	Minimum: -90deg Maximum: 90deg Sampling step: 10deg	Minimum: 0m Maximum: Road Width Sampling step: 0.1m
	4m				
	3.5m				

B. Results and Discussions

Results demonstrate that the proposed motion planner is: i) with the function of mirroring the parking target; ii) enhancing parking success rate by 40.6%; iii) expanding ODD by 86.1%; iv) reducing 47.6% number of driving direction switching and 18.0% parking time duration; v) with 74 milliseconds of average computation time.

1) Function Validation Results

The function of mirroring the parking target is verified in Fig. 17. It illustrates the planned trajectories and the real parking trajectories in all three types of parking scenarios. The planned trajectories are towards a mirrored parking target. By executing negative control commands after the mirror line, the vehicle can park into the slot successfully.

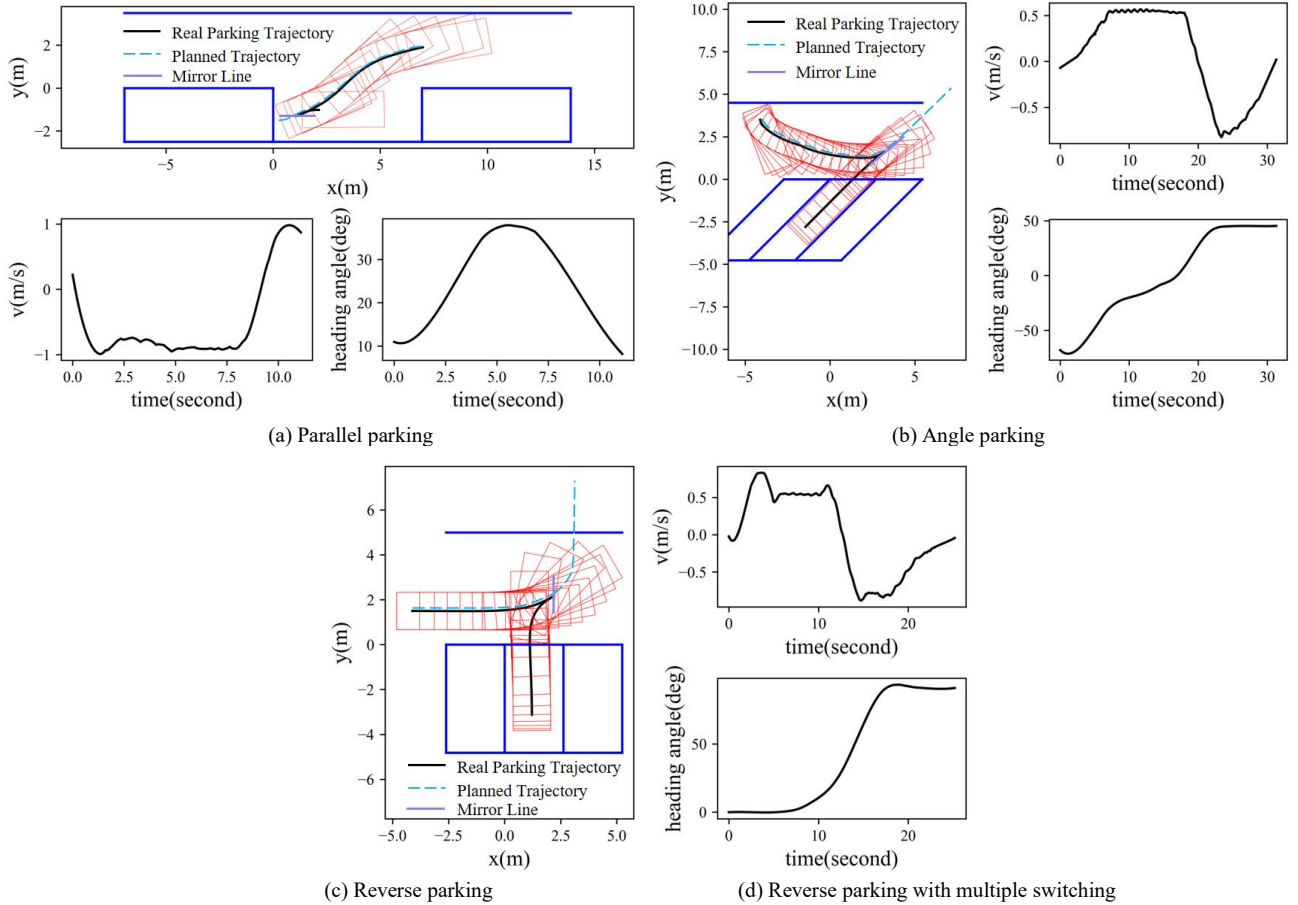


Fig. 17. Parking trajectory examples

2) Parking Capability in Narrow Spaces Results

The proposed planner is able to enhance parking capability by 40.6%, compared to the baseline controller. The parking capability is quantified by parking success rate, as illustrated in Fig. 18. It shows that the proposed motion planner is with greater parking success rate in all parking types.

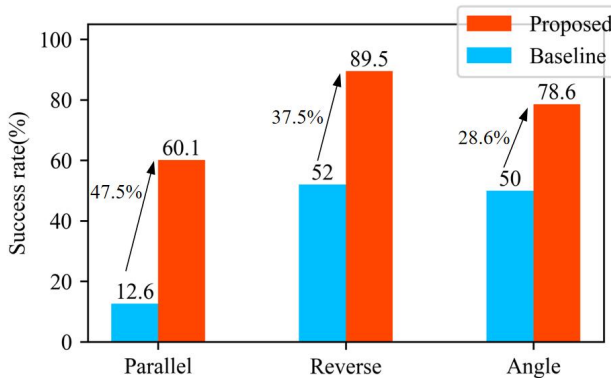


Fig. 18. Success rate results

The proposed planner particularly shows its superiority in more difficult cases. First, the proposed planner has greater enhancement on parking capability in difficult parking types, like parallel parking [28]. As shown in Fig. 18, the parking success rate enhancement in parallel parking is 47.5%. It is significantly greater than the enhancement in reverse parking and angle parking. Second, the proposed planner has greater enhancement on parking capability in narrower spaces. As shown in Fig. 19, the parking success rate enhancement increases with the decrease of road width. It is because the proposed planner barely deteriorates with the decrease of road width, as shown in Fig. 19. It is able to take extreme measures to find a way to squeeze into the parking slot. An example trajectory is provided in Fig. 20. In this case, the proposed planner made over many direction switches, and finally accomplished its parking process. While, the baseline planner attempts to search for a path directly leading towards the parking slot. Due to its greedy nature, all the attempts failed as the shorter paths are more likely constrained by the narrower spaces.

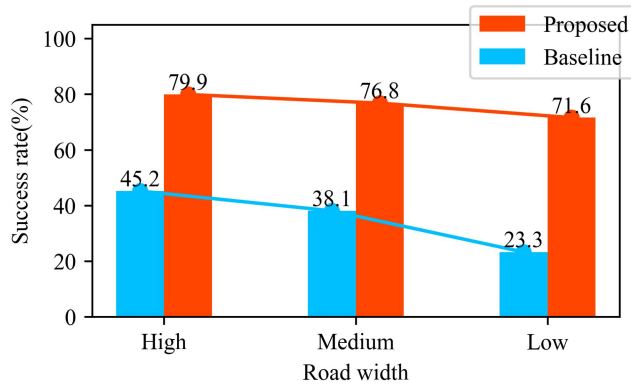


Fig. 19 Success rate VS road width

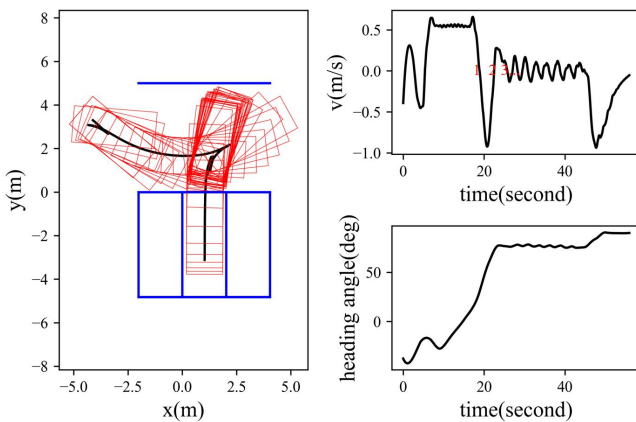


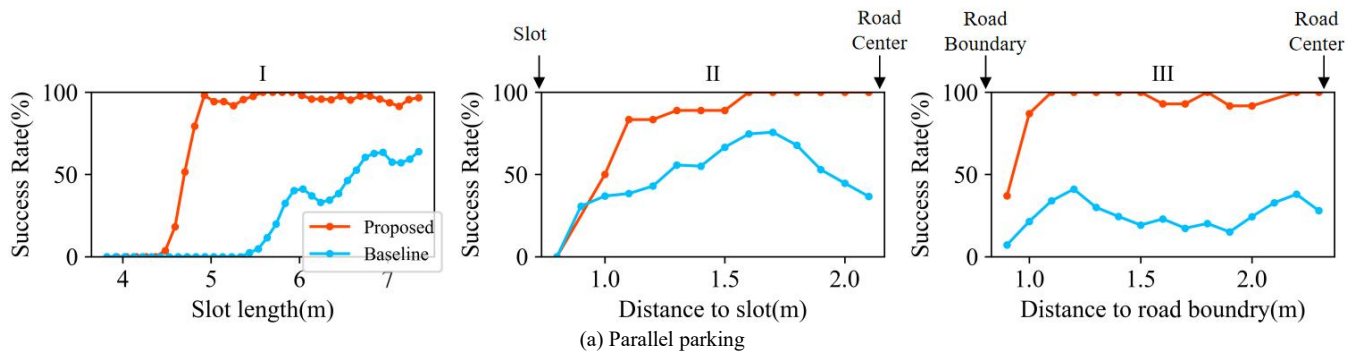
Fig. 20 Example of parking capability in narrow spaces

The result of sensitivity analysis of parking capability in terms of slot size is shown in the column I of Fig. 21. It demonstrates that the proposed planner enhances parking capability. The enhancement is particularly significant with a narrower parking slot. The magnitude of the enhancement becomes increasingly significant as slot size decreases. This confirms the proposed planner's parking capability in narrow spaces. It is discovered that the baseline planner cannot ensure a 100% parking success rate regardless of space sizes in parallel parking. This is in line with daily experiences that

parallel parking is the most difficult parking type. For people, that are able to handle reverse parking and angle parking, cannot always complete a parallel parking. Nevertheless, the proposed planner can handle parallel parking as good as the other two parking types. This confirms the robustness of the proposed planner.

It is interesting to find that the success rate of the conventional planner does not increase linearly with slot size. Take angle parking as an example, the success rate remains constant when the slot width is around 2 meters. It is due to the nature of the baseline planner, as it needs to complete the final path by connecting towards the parking slot with a predetermined curve. Since the curve is selected from a fixed library, the degree of freedom is limited around the final path. Hence, there are chances that two adjacent positions could have two significantly different success rates. This causes the success rate not always continuously increase with slot size. This is not the case for the proposed planner. By mirroring the parking target, the proposed planner is able to perform global optimizations and make the most of the space available. Therefore, any increment in slot size leads to a gain in success rate. This again confirms the superiority of the proposed planner when dealing with narrow parking slots.

The result of sensitivity analysis of parking capability in terms of vehicle's initial position is shown in the column II and III of Fig. 21. Result shows that parking success rate increases with the free space around the initial position. It is confirmed by the column II of Fig. 21 that success rate is higher when the vehicle's initial position is farther from the slot. It is confirmed again by the column III of Fig. 21 that success rate is higher when the vehicle's initial position is farther from the road boundary. However, the success rate does not always increase with the space available. It reaches the maximum success rate of around 100% when the distance to slot is over 1.6 meters, as there is simply no room for further improvement. Therefore, to achieve the best user experience, future users are suggested to activate the system after placing their vehicles at least 1.6 meters away from the slot.



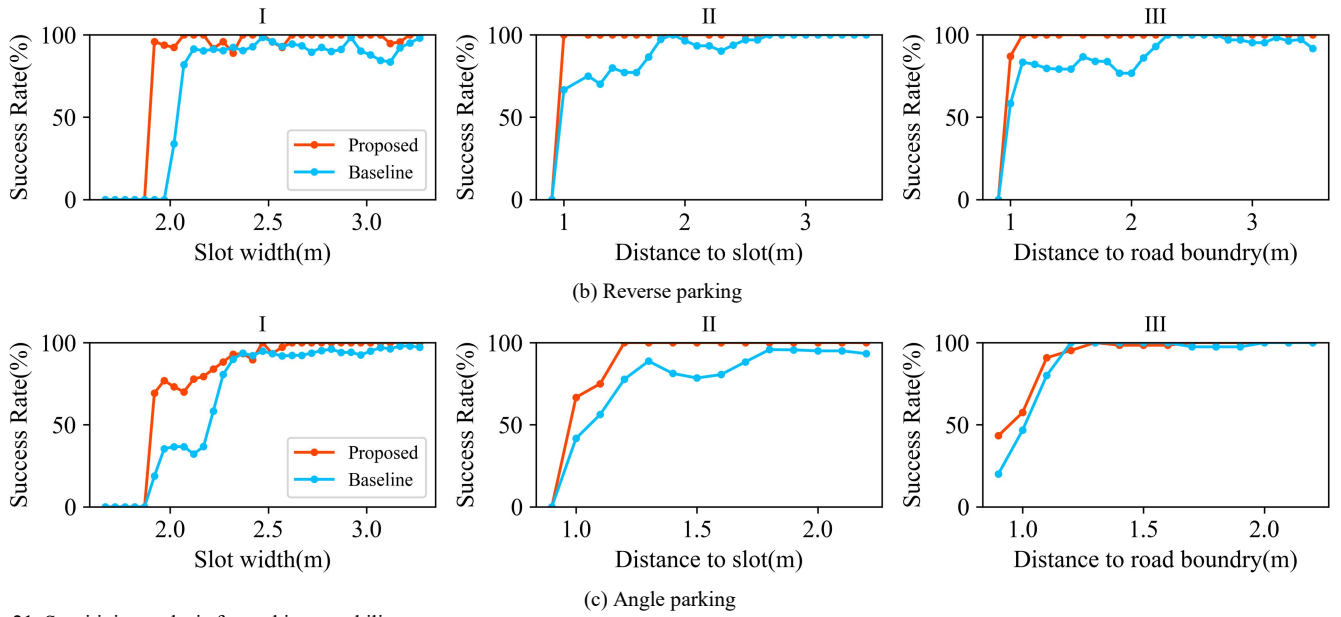
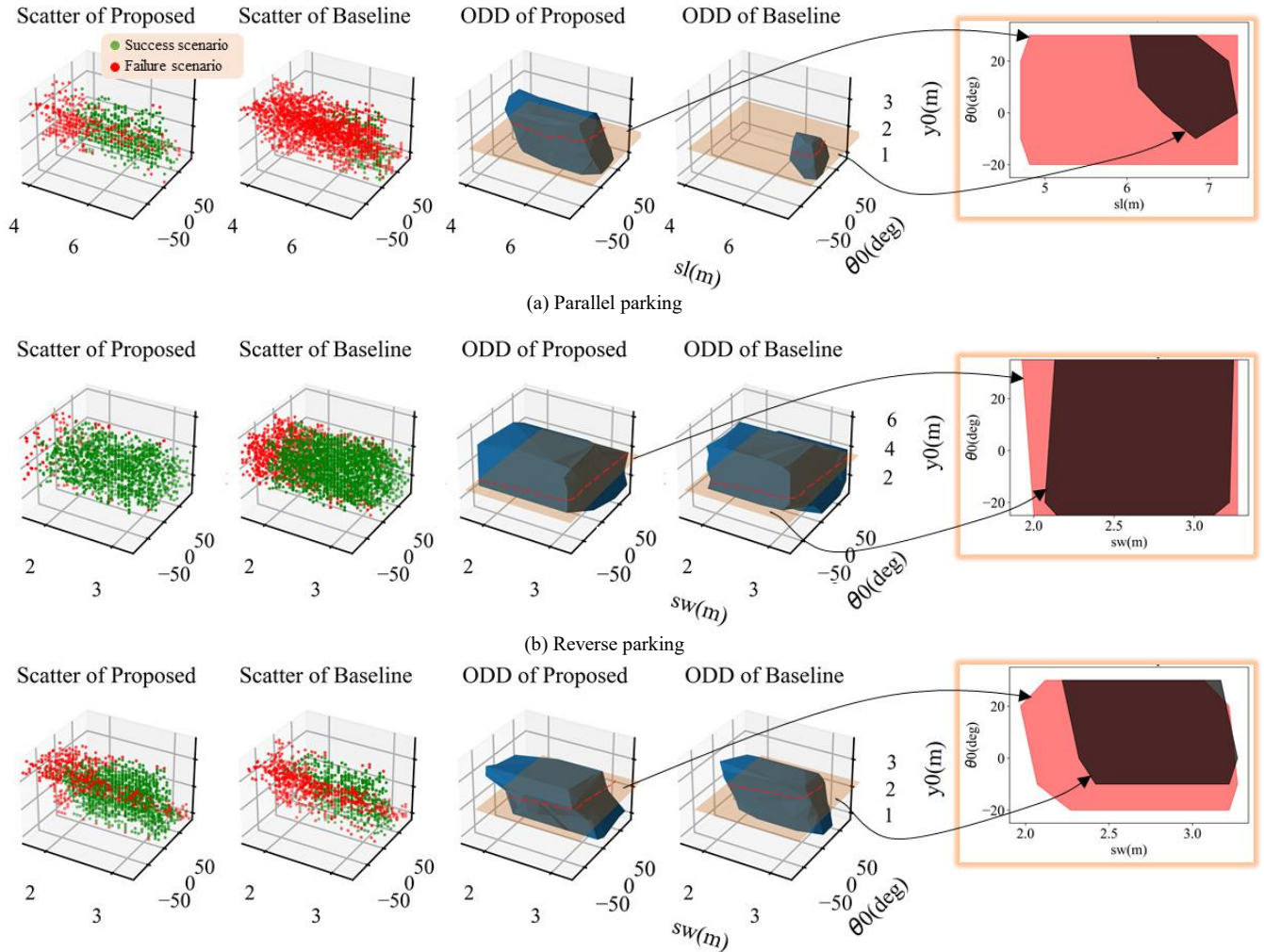


Fig. 21. Sensitivity analysis for parking capability

3) Parking reliability Results

The proposed planner is confirmed with greater parking reliability. Parking reliability is quantified by ODD, as shown in Fig. 22. Green nodes are the successful cases. Red nodes are the failed cases. ODD is the collection of green nodes. It

shows that the proposed planner expands the ODD by 86.1%, compared to the baseline planner. Therefore, the proposed planner is able to handle a greater variety of parking slots and conditions. This indicates its greater commercial implementation potential.



(c) Angle parking

Fig. 22. The scatter plot of parking results and its ODD representation

4) Parking Completion Efficiency Results

The proposed motion planner is with greater parking completion efficiency compared to the baseline. The parking completion efficiency has been quantified by the number of driving direction switching and parking time duration, as illustrated in Fig. 23. As shown by the left plots in Fig. 23, the

proposed planner reduces 47.6% direction switchings. The average direction switching number is only 3.3. As shown by the right plots of Fig. 23, the proposed planner reduces parking time duration by 18.0%. It needs 28.2 seconds on average to finish a parking.

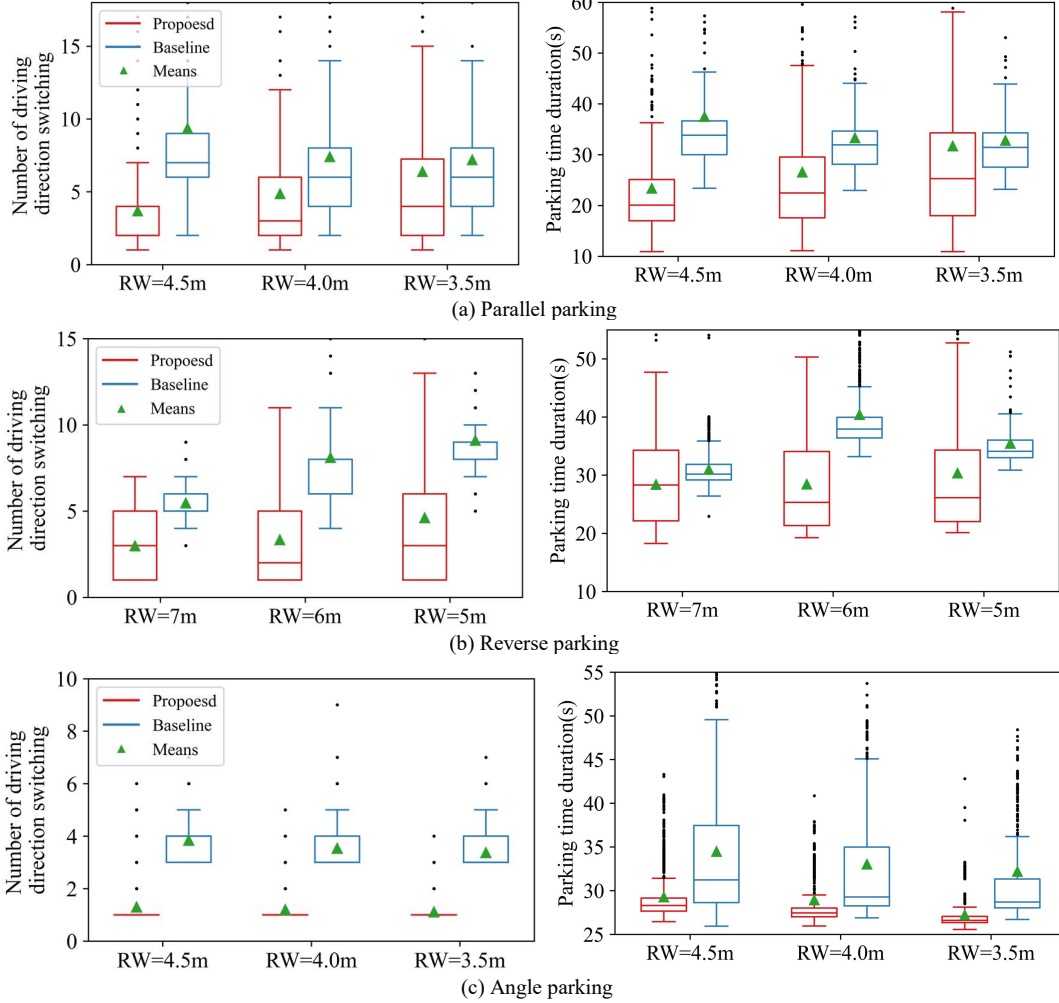


Fig. 23. Parking performance results

5) Computation Efficiency Results

The proposed planner enhances computation efficiency by 95.8% compared to the baseline. When running on a laptop equipped with an Intel i7-9750H CPU, the average computation time of the proposed motion planner is only 74 milliseconds. While, the average computation time of the baseline planner is 1.8s. Consequently, the proposed motion planner is with the potential of real-time implementation.

IV. CONCLUSION AND FUTURE RESEARCH

This research proposes an optimal-control-based parking motion planner. Its highlight lies in its control logic: planning trajectories by mirroring the parking target. This method enables: i) parking capability in narrow spaces; ii) better parking reliability by expanding ODD; iii) faster completion of parking process; iv) enhanced computational efficiency; v)

universal to all types of parking. A comprehensive evaluation is conducted by simulation. Results demonstrate that:

- The proposed planner does enhance parking success rate by 40.6%, improve parking completion efficiency by 18.0%, and expand ODD by 86.1%;
- The proposed planner shows its superiority in difficult parking cases, such as the parallel parking scenario and narrow spaces;
- Users are advised to activate the proposed system after placing their vehicles at least 1.6 meters away from the slot. In this way, an 100% success rate could be guaranteed;
- The average computation time of the proposed planner is 74 milliseconds. It indicates that the proposed planner is ready for real-time application.

In this research, parking completion efficiency is the priority. Future research could consider and balance more parking objectives.

REFERENCES

- [1] "Automotive Intelligence Park Assist System Market Report ", [Online]. Available: <https://www.fortunebusinessinsights.com/automotive-intelligence-e-park-assist-system-market-106398>.
- [2] "Automated Parking Assist (APA) and Automated Valet Parking (AVP) Industry Report, 2021," [Online]. Available: <https://www.globenewswire.com/news-release/2021/05/20/2233500/0/en/Automated-Parking-Assist-APA-and-Automated-Valet-Parking-AVP-Industry-Report-2021.html>.
- [3] "Driver Interactive Vehicle Experience Report," [Online]. Available: <https://www.jdpower.com/business/press-releases/2015-driver-in-teractive-vehicle-experience-drive-report>.
- [4] W. Wang, Y. Song, J. Zhang, and H. Deng, "Automatic parking of vehicles: A review of literatures," *International Journal of Automotive Technology*, vol. 15, pp. 967-978, 2014.
- [5] K. Lee, D. Kim, W. Chung, H. W. Chang, and P. Yoon, "Car parking control using a trajectory tracking controller," in *2006 SICE-ICASE International Joint Conference*, 2006: IEEE, pp. 2058-2063.
- [6] P. Zhang *et al.*, "Reinforcement learning-based end-to-end parking for automatic parking system," *Sensors*, vol. 19, no. 18, p. 3996, 2019.
- [7] H. Li, Y. Luo, and J. Wu, "Collision-free path planning for intelligent vehicles based on Bézier curve," *IEEE Access*, vol. 7, pp. 123334-123340, 2019.
- [8] Z. Liang, G. Zheng, and J. Li, "Automatic parking path optimization based on bezier curve fitting," in *2012 IEEE International Conference on Automation and Logistics*, 2012: IEEE, pp. 583-587.
- [9] T. Fraichard and A. Scheuer, "From Reeds and Shepp's to continuous-curvature paths," *IEEE Transactions on Robotics*, vol. 20, no. 6, pp. 1025-1035, 2004.
- [10] P. Soueres and J.-P. Laumond, "Shortest paths synthesis for a car-like robot," *IEEE Transactions on Automatic Control*, vol. 41, no. 5, pp. 672-688, 1996.
- [11] Z. Qin, X. Chen, M. Hu, L. Chen, and J. Fan, "A novel path planning methodology for automated valet parking based on directional graph search and geometry curve," *Robotics and Autonomous Systems*, vol. 132, p. 103606, 2020.
- [12] J.-H. Jhang and F.-L. Lian, "An autonomous parking system of optimally integrating bidirectional rapidly-exploring random trees* and parking-oriented model predictive control," *IEEE Access*, vol. 8, pp. 163502-163523, 2020.
- [13] A. R. Soltani, H. Tawfik, J. Y. Goulermas, and T. Fernando, "Path planning in construction sites: performance evaluation of the Dijkstra, A*, and GA search algorithms," *Advanced engineering informatics*, vol. 16, no. 4, pp. 291-303, 2002.
- [14] J. Lai, J. Hu, L. Cui, Z. Chen, and X. Yang, "A generic simulation platform for cooperative adaptive cruise control under partially connected and automated environment," *Transportation Research Part C: Emerging Technologies*, vol. 121, p. 102874, 2020.
- [15] H. Wang, J. Lai, X. Zhang, Y. Zhou, S. Li, and J. Hu, "Make space to change lane: A cooperative adaptive cruise control lane change controller," *Transportation Research Part C: Emerging Technologies*, vol. 143, p. 103847, 2022.
- [16] M. Gyllenhammar *et al.*, "Towards an operational design domain that supports the safety argumentation of an automated driving system," in *10th European Congress on Embedded Real Time Systems (ERTS 2020)*, 2020.
- [17] R. Rajamani, *Vehicle dynamics and control*. Springer Science & Business Media, 2011.
- [18] J. Hu, Z. Zhang, L. Xiong, H. Wang, and G. Wu, "Cut through traffic to catch green light: Eco approach with overtaking capability," *Transportation research part C: emerging technologies*, vol. 123, p. 102927, 2021.
- [19] J. Hu, H. Wang, Y. Feng, and X. Li, "Optimal Control-Based Highway Pilot Motion Planner With Stochastic Traffic Consideration," *IEEE Intelligent Transportation Systems Magazine*, 2022.
- [20] J. Hu, Y. Feng, X. Li, and H. Wang, "A Model Predictive Control Based Path Tracker in Mixed-Domain," in *2021 IEEE Intelligent Vehicles Symposium (IV)*, 2021: IEEE, pp. 1255-1260.
- [21] G. Codato and M. Fischetti, "Combinatorial Benders' cuts for mixed-integer linear programming," *Operations Research*, vol. 54, no. 4, pp. 756-766, 2006.
- [22] L. Gurobi Optimization, "Gurobi optimizer reference manual," ed, 2018.
- [23] J. Hu, S. Sun, J. Lai, S. Wang, Z. Chen, and T. Liu, "CACC Simulation Platform Designed for Urban Scenes," *IEEE Transactions on Intelligent Vehicles*, 2023.
- [24] D. Dolgov, S. Thrun, M. Montemerlo, and J. Diebel, "Practical Search Techniques in Path Planning for Autonomous Driving," *Ann Arbor*, vol. 1001, p. 48105, 2008.
- [25] ISO16787:2017(E): *Intelligent transport systems-Assisted parking system (APS)- Performance requirements and test procedures*.
- [26] ISO 20900:2019: *Partially automated parking systems (PAPS) — Performance requirements and test procedures*.
- [27] L. Xue, Y. Leng, and X. Lian, "Automotive Parking Assistant Testing Scene analysis and evaluation research," in *Journal of Physics: Conference Series*, 2021, vol. 1873, no. 1: IOP Publishing, p. 012079.
- [28] J. Song, W. Zhang, X. Wu, H. Cao, Q. Gao, and S. Luo, "Laser-based SLAM automatic parallel parking path planning and tracking for passenger vehicle," *IET Intelligent Transport Systems*, vol. 13, no. 10, pp. 1557-1568, 2019.